LBNL-48978

To be submitted to the
Journal of Applied Physics

Ion flux from vacuum arc cathode spots in the absence and presence of a magnetic field

André Anders[*1)] and George Yu. Yushkov[2)]
1) Lawrence Berkeley National Laboratory, University of California,
1 Cyclotron Road, MS 53, Berkeley, California 94720, USA.
2) High Current Electronics Institute, Russian Academy of Sciences, Tomsk 634055, Russia.

March-September 2001

Corresponding Author:
André Anders
Lawrence Berkeley National Laboratory
1 Cyclotron Road, MS 53-004
Berkeley, CA 94720, USA
Tel. + (510) 486-6745
Fax + (510) 486-4374
e-mail aanders@lbl.gov

This work was supported by the U.S. Department of Energy, Office of Energy Research, under Contract No. DE-AC03-76SF00098, and by the Russian Foundation for Basic Research, under Grant No. 99-02-18163.

[*] Corresponding Author, aanders@lbl.gov

Ion flux from vacuum arc cathode spots in the absence and presence of a magnetic field

André Anders[*1)] and George Yu. Yushkov[2)]

1) Lawrence Berkeley National Laboratory, University of California,
1 Cyclotron Road, MS 53, Berkeley, California 94720, USA.

2) High Current Electronics Institute, Russian Academy of Sciences, Tomsk 634055, Russia.

Abstract

Because plasma production at vacuum cathode spots is approximately proportional to the arc current, arc current modulation can be used to generate ion current modulation that can be detected far from the spot using a negatively biased ion collector. The drift time to the ion detector can used to determine kinetic ion energies. A very wide range of cathode materials have been used. It has been found that the kinetic ion energy is higher at the beginning of each discharge and approximately constant after 150 μs. The kinetic energy is correlated with the arc voltage and the cohesive energy of the cathode material. The ion erosion rate has in inverse relation to the cohesive energy, enhancing the effect that the power input per plasma particle correlates with the cohesive energy of the cathode material. The influence of three magnetic field configurations on the kinetic energy has been investigated. Generally, a magnetic field increases the plasma impedance, arc burning voltage, and kinetic ion energy. However, if the plasma is produced in a region of low field strength and streaming into a region of higher field strength, the velocity may decrease due to the mirror effect. A magnetic field can increase the plasma temperature but may reduce the density gradients by preventing free expansion into vacuum. Therefore, depending on the configuration, a magnetic field may increase or decrease the kinetic energy of ions. Additionally, the angular distribution of the ion flux and ion kinetic energy has been investigated in the absence of an external magnetic field. The result can be fitted by a superposition of an isotropic and a cosine distribution.

[*] Corresponding Author, aanders@lbl.gov

I. INTRODUCTION

It is well-known that the vacuum arc plasma is produced at non-stationary cathode spots– locations of micron-size, characterized by extremely high current density, power density, and plasma density[1-5]. The cathode material is the feedstock material for the plasma. It is also well known that the velocity of ions is very high, of order 10^4 m/s, and hence supersonic with respect to the ion sound velocity[6].

Due to the small dimensions of the arc cathode spot, and the highly non-stationary nature with characteristic times down to the nanosecond time scale, measurements have been difficult and interpretation often quite controversial. Today it is recognized that the plasma pressure in the spot exceeds atmospheric pressure by orders of magnitude and thus the presence of gas affects spot processes only indirectly. Therefore, although we focus here on the ion flux from *vacuum* arc cathode spots, the ion flux from arc cathode spots in gases should be included in the discussion, at least from a historical point of view. Measurements of ion velocities from cathode spots can be traced back to the late 1800s, i.e. to a time when neither good vacuum was available nor plasma particles such as ions and electrons were known. For instance, Schuster[7] determined a zinc velocity in air averaged over the first 1 mm from the cathode surface to about 2000 m/s using spectroscopic methods and a camera with a rapidly rotating mirror similar to that developed by Feddersen[8] in 1861.

Tanberg[9] published first velocity data for vacuum arc copper ions in 1930. He measured $\bar{v}_i(\mathrm{Cu}) = 1.6 \times 10^4$ m / s using two indirect methods: the reaction force of the plasma on the cathode, and the force of the plasma on a suspended vane. Tanberg's result was surprisingly accurate, as confirmed by later measurements using the same and other methods such as retarding field analyzers [10,11]. The latter works contain also data for numerous other elements; all velocities were found to be in a relatively narrow range $0.5 - 3 \times 10^4$ m / s, with the low mass-ions being faster than the high-mass ions. Earlier work indicated that there is a slight dependence of the ion velocity on the ion charge state which lead to the assumption of the "potential hump" hypothesis according to which ions are accelerated by the electric field of the hump[10,11]. More recent velocity measurements using current-perturbation methods show that the ion velocities in vacuum arcs are practically independent of charge states [6,12,13]. Consequently, a hydrodynamic ion acceleration mechanism seems to be responsible for the high ion velocities.

The current-perturbation methods are based on a perturbation of ion generation via the arc discharge current and the measurement of the time-of-flight for the perturbation to arrive at a detector. Ions can be extracted from the plasma allowing researchers to combine the time-of-flight measurement in the plasma with the charge-state-resolving time-of-flight (TOF) method in the ion beam[6,12,13].

The perturbation can be a "current jump[12]," or "spike[13]," or a sequence of spikes[14], or the forced rapid extinction of the arc discharge[15], or a "gentle" modulation of the arc current[6]. The latter has the advantage that the perturbation has only a minor effect on the arc voltage, power balance, ion charge state distribution, ion velocity and other parameters. Therefore, we will use the relatively gentle current modulation approach in this work.

Recent measurements[6] using Berkeley's vacuum arc ion source facility "Mevva V"[16] determined that the ion velocities are in the range 0.42 - 3.0 x 10^4 m/s, depending on the material. Using ion velocities one may find the corresponding ion Mach numbers which are defined as the ratio of the ion velocity to the ion sound speed[17]

$$v_{is} = \sqrt{\frac{\gamma_e kT_e + \gamma_i kT_i}{m_i}} \quad , \tag{1}$$

with $\gamma_e \approx 1$ (isothermal electrons) and γ_i between 5/3 (adiabatic ions, many collisions) and 3 (adiabatic ions, absence of collisions). The ion sound speed can be estimated using the temperature derived from ion charge state measurements[18]. The arc current, as given by the circuit, and the self-adjusting burning voltage determine the energy input and the characteristic plasma parameters. As was experimentally shown[19], the material specific burning voltage has a surprisingly simple, linear relation to the cohesive energy of the cathode material ("Cohesive Energy Rule"[20]). In this paper we expand the research on ion velocities and other ion flux parameters to address the following issues:

- cross-check the perturbation measuring principles using this time a plasma probe as the ion detector, while covering a wide range of cathode materials,
- determine effects of a magnetic field, if any, on the ion kinetic energies,
- determine possible correlation between arc burning voltage and ion kinetic energies as a function of the magnetic field amplitude and field distribution,
- measure angular ion flux distributions, and
- quantify the relation, if any, between ion flux and cohesive energy.

II. MEASURMENT PRINCIPLE AND EXPERIMENTAL DETAILS

Several experimental setups were used to address the wide range of issues mentioned above. Figure 1 shows the first setup that is essentially comprised of modified "Mevva V" ion source components, with the ion extraction system removed. The arc discharge occurred between the front face of a cylindrical cathode of 6.25 mm diameter and an annular anode of 1.3 cm inner diameter. The closest cathode-to-anode distance was about 5 mm.

A pulsed, axial magnetic field could optionally be used. The field coil was positioned such as to magnetically insulate the anode thereby increasing the arc burning voltage (Fig 1; for more details see figure 1 of Ref.[21]). The field coil, if used, was powered by discharging a capacitor bank of 250 μF via a thyristor switch that was synchronized with the arc pulse. The coil current reached its maximum 140 μs after triggering the thyristor, and decreased exponentially with a time constant of about 0.5 ms. The magnetic field strength was measured with a calibrated pickup coil. The magnetic field strength is non-uniform along the plasma's drift path; we quote the magnetic field strength at the position of the cathode surface, the plasma's "place of birth." The magnetic field in the center of the coil is stronger by a factor of 2.2.

The arc discharge was fed by an 8-stage pulse-forming-network (PFN) of 1 □ impedance delivering a nearly rectangular arc pulse shape of 250 μs duration and 100-500 A amplitude depending on the charging voltage. The arc current was modulated by adding an L-C branch to the PFN as shown in Figure 1.

The vacuum chamber was cryogenically pumped to a base pressure of about 10^{-4} Pa.

In contrast to previous measurements where the ion extraction feature of the system was used, the ion current modulation was detected by a Langmuir probe working in the ion saturation regime with a constant negative bias of -60 V. Because ion acceleration occurs in the vicinity (< 1 mm) of the cathode spot[22,23], the ion velocity can be treated as constant for the length of the drift region between the cathode and the sheath edge of the detecting probe (s=277 mm in most experiments). The ion velocity is simply

$$v_i = s / t_{pl} \quad . \tag{2}$$

and the ion energy

$$E_i = m_i \, v_i^2 / 2 \tag{3}$$

where t_{pl} is the time of flight of ions in the plasma drift region as measured by the time delay between an arc current maximum (or minimum) and the corresponding ion current maximum (or minimum). Figure 2 illustrates such a delay time measurement. The method is based on the assumption that ion production is approximately proportional to the arc current and the plasma streaming velocity "far" from the spot (> 1 mm) is constant. Both assumptions are well supported by the vast vacuum arc literature. The delay time error introduced by acceleration of ions in the sheath of the probe is negligible because of the sheath thickness is small[24].

Because the measuring principle is simpler than previous perturbation methods where ion extraction was used, we expect results to be more reliable. However, while previous experiments allowed us to distinguish between ions of different charge states, one needs to realize that here we only obtain data averaged over all ion charge states - the price we pay for greater simplicity and reliability.

III. EXPERIMENTAL RESULTS

A. Ion flux measurements without external magnetic field

For these measurements described next, the magnetic field coil was not activated. The delays between corresponding arc and ion current maxima and minima (Fig.2) were measured in order to determine whether or not the velocity is approximately constant throughout the arc pulse. As shown in Figure 3, we found the highest velocity at the beginning of each arc pulse. Steady-state values are practically obtained after about 150 μs. The arc burning voltage shows a similar decay from high values at the beginning to steady-state -- a fact that is not coincidental, as discussed in section IV. One needs to keep in mind, however, that curves shown in figures 2 and 3 are obtained by averaging over many (e.g. 16) arc pulses; the individual voltage and ion current curves are characterized by fluctuations caused by the explosive nature of plasma formation at cathode spots[4]. Averaging allows us to determine an average ion velocity at a given time after arc ignition.

The time delays between arc current and ion current were determined for a large number of cathode materials. Averaged steady-state velocities determined this way are compiled in Table 1. These and the other data of Table 1 are discussed in section IV.

In conjunction with the ion velocity, the arc burning voltage was measured using a voltage divider as shown in figure 1. The average data for quasi-steady-state conditions (t > 150 μs) are also included in Table 1. As anticipated from energy considerations[20] and detected in previous data[25], the arc burning voltage and the kinetic energy are correlated as shown in figure 4.

Yet another interesting result follows from the values of ion currents measured by the probe. Although we did not focus on this issue, the probe currents can be used to determine relative ion erosion rates. The ion erosion rate can be defined as the mass loss of the cathode in form of ions normalized to the charge flowing through the cathode, i.e.

$$\Gamma_i = N_i A \Big/ \int_0^{\tau} I_{arc} \, dt \tag{4}$$

with N_i the number of ions of atomic mass number A produced during the time τ by an arc of current amplitude I_{arc}. If we assume that the ion flux distribution is independent of the ion mass, the ion current measured by the ion collector (having a relatively small spatial angle) divided by the known average charge state[16] gives relative ion erosion rates (Fig. 5).

B. Ion velocity measurements with external magnetic field of the "Mevva V" configuration

It has been shown that an external magnetic field influences the discharge and plasma properties such as ion charge state distributions[26]. From energy considerations it can be anticipated that the ion velocity is affected by a magnetic field in a similar manner. The input power to the arc discharge is

$$P_{arc} = I_{arc} V_{arc} \tag{5}$$

The arc current is determined by the impedance of the circuit because the impedance of the plasma is much smaller than the impedance of the rest of the circuit. The arc input power is therefore a function of the self-adjusting arc burning voltage V_{arc}, i.e. the potential difference between cathode and anode which should not to be confused with the open-circuit charging voltage of the circuit. Burning voltage[27] and ion charge distributions[16] were previously obtained at the "Mevva V" ion source; so it was reasonable to measure ion velocities using the same facility and thus have sets of data that can easily be linked and compared. For these experiments, the field coil shown in figure 1 was activated. The most relevant results are compiled in figures 6 and 7. These figures show that the arc burning voltage and the kinetic energy of ions increase with increasing magnetic field but both increases have a tendency to level off toward saturation, similar to what has been previously observed with the mean ion charge state as a function of magnetic field[26]. To check a possible direct proportionality of arc voltage and ion velocity, both quantities are plotted against each other in figure 8 – the result will be discussed in section IV.

C. Ion velocity measurements with other external magnetic field configurations

These results of section II B are valid for a fixed configuration of the magnetic field as shown in figure 1. The *strength* of the field could be varied but one also needs to consider the field gradients with respect to the cathode-anode discharge gap. Therefore additional experiments were performed in a different chamber allowing us to change the field geometry to configurations other than the "Mevva V" configuration. As shown in figure 9, there were two field coils that could be operated individually or collectively. The short coil, wound around the grounded anode, consisted of 60 turns of insulated copper wire over a length of 20 mm, with an average coil diameter of 30 mm. The second coil was very long, 480 mm, consisting of 96 turns of copper wire, wound on a plastic tube that enclosed a grounded stainless steel tube of 70 mm diameter and 500 mm length. The field strengths (normalized to the coil current) of the short and long coil were measured with a calibrated pick-up coil, giving 0.49 mT/A and 0.041 mT/A in the center of each coil, respectively. When both coils were powered, the field strength at the cathode was 0.54 mT/A. The choice of the magnetic field configuration was made such that when the plasma was produced in the center of the short coil it would expand only into space of decreasing field strength, while it would drift in a constant field region when only the long coil was powered.

Depending on the field configuration, the kinetic energy of ions far from the spot depends not only on the field strength but also on the field and discharge configuration. As figure 10 shows, the ion energy can increase when the plasma is expanding into a region of lower field, decrease when decelerated in an initially increasing field, or a show a non-monotonic behavior.

D. Measurements of the angular ion current density distribution

All of the above measurements were performed such that the plasma flux normal to the surface was investigated. It is known that the arc plasma plumes preferentially around the surface normal and thus it is desirable to obtain information about the angle dependence of ion energy and other plasma parameters.

The experimental setup for this experiment is shown in Figure 11. A rotatable vacuum arc cathode assembly was placed in the center of a round vacuum chamber of 1 m diameter. The assembly could be turned by 180° without interrupting vacuum. As in the other experiments, the cathode was rod of 6.25 mm diameter mounted in an alumina sleeve such as to confine the area of cathode spot activity to its front surface. The grounded wall of the vacuum chamber served as the anode. A negatively biased probe was located 350 mm from the cathode surface to operate as a time-resolving ion current collector. Using the arc and ion current modulation technique, the results compiled in figures 12 and 13 have been obtained. Figure 12 indicates that the ion velocity or kinetic energy is maximum for the surface normal and reduced with increasing angle with respect to the surface normal. Using the ion saturation current measured by the probe, the ion particle flux can be plotted a function of angle as shown in figure 13.

IV. DISCUSSION

A. Ion flux properties in the absence of an external magnetic field

The perturbation method using "gentle" current oscillations and a negatively biased ion collector appears as a simple yet powerful experimental approach to measure ion velocities and other ion flux parameters. Because of its simplicity, interpretation of data is relatively straightforward.

In figure 14, ion velocity data in the absence of external magnetic field are compared with hydrodynamic models (see below). One can notice that there is surprisingly good agreement. Earlier measurements[6] where the ion extraction system of the "Mevva V" ion source was used gave similar results with the exception for light elements where higher velocities were found. Based on the simplicity argument for the present measurements, and the good agreement with other literature data (e.g.[10]) and hydrodynamic formulas, we believe that there must have been a systematic error for the light elements in the previous measurements[6]. The nature of the systematic shift is not clear but it may be associated with the ion optics of the extraction system.

The error of the measurements presented here is about ±10% resulting from the accuracy of determining the time difference between extrema of oscillations of arc current and ion current. This accurany was considered sufficient because the distributions are broad and subject to fast fluctuations. The general validity of the average values may slightly depend on the specifics of the electrode size, position, temperature, and similar details, and thus we estimate that other configurations may give average data that deviate by as much as 25%.

Ion acceleration to supersonic velocity has been discussed many times in the literature, e.g. Ref.[2,5,10,22,23,25,28,29]. Here we limit ourselves to one-dimensional, spherical hydrodynamic models because they provide simple physical interpretation and formulas that agree surprisingly well with experimental data. Assuming that all energy is deposited in the two-fluid plasma in a cathode spot volume that is much smaller than the expansion region, and considering adiabatic expansion, Litvinov[28] and Mesyats and Proskurovsky[2] derived the expression

$$v_i \approx \frac{2}{\gamma - 1}\sqrt{\gamma \frac{kT_i^* + \overline{Q}\ kT_e^*}{m_i}} \tag{6}$$

for the final ion velocity, where $\gamma \approx 5/3$ is the adiabatic coefficient and the star indicates the initial temperature in the cathode spot. Similarly, Krinberg[30-32] considered a multi-component plasma and solved the equations of energy and motion leading to the simple approximate expression

$$v_i \approx 3.5\sqrt{\overline{Q}\ kT_e^*/m_i} \tag{7}$$

where T_e^* denotes the electron temperature at the critical point where ion velocity becomes supersonic. To evaluate these formula, one may use the temperature data[18] that have been derived from measured ion charge state distributions[16]. The charge state distributions "froze" very close to the cathode spot, thereby preserving the temperature information to the expanded plasma region far from the spot where measurements were possible[33]. The temperature data are included in Figure 15, which is further discussed below.

Although the ion velocities give important clues about the physical mechanisms underlying cathode spot operation and ion acceleration, one must keep in mind that that these data represent average values. Indeed, averaging occurs in several dimensions. One average is over the charge states because we do not resolve charge states with the simple approach presented here. Experimental data from previous years indicate that this is permissible because there was very little difference between the velocities of different charge states[6,34]. Additionally, the measurements average over fast fluctuations. Limited time resolution was attempted by selecting different maxima and minima after arc initiation (Fig. 2) but fluctuations faster than a few microseconds were not resolved. In fact, for better precision of the average velocity, averaging over at least 16 measurements for each data point was performed. Finally, ions have a velocity *distribution* and thus data here represent an average over the distribution.

According to the "cohesive energy rule,"[35] the arc voltage increases linearly with the cohesive energy E_{CE} of the cathode material following the relation

$$V_{arc} = V_0 + A\, E_{CE} \tag{8}$$

where the constants for our experimental setup were found to be $V_0 \approx 14$ V and $A = 1.69$ V / (eV / atom).

This suggests to look for a similarly simple relationship for the ion kinetic energy. Figure 15 shows that one can find a correlation between the ion kinetic energy and cohesive energy. A linear fit of the type

$$E_{kin} = E_{kin0} + B\, E_{CE} \tag{9}$$

gives $E_{kin0} \approx 5.2 \pm 7.4$ eV and $B \approx 13.7 \pm 1.6$ with a correlation coefficient 0.81. This coefficient is relatively far from unity indicating that the distribution of input energy to the various output energy channels (kinetic energy, ionization energy, radiation, energy in macroparticles, etc) is indeed complex.

As shown in figure 5, a greater cohesive energy of the cathode material leads to reduced ion erosion rates. One may conclude that the *total* erosion rate correlates with the cohesive energy due to the direct relationship between cohesive energy and melting and boiling temperature on the one hand[19] and macroparticle size and melting temperature on the other hand[36,37]. A smaller erosion rate at a given power input provides more power per plasma particle, leading to higher temperature, ion charge state, and velocity for materials of high cohesive energy. It will also lead to greater momentum that each ion has. Momentum data are included in Table 1. Ion momentum is of relevance for energetic deposition of thin films and for the efficiency of vacuum arc thrusters that may be used for space propulsion of satellites.

B. Ion flux properties in the presence of an external magnetic field

If an external magnetic field is applied, electrons emitted from the cathode have to move across magnetic field lines to reach the anode ("magnetic insulation" of the anode). The impedance of the discharge is enhanced, leading to higher burning voltage (Figure 7) and power input according to equation (5). It is known that higher input power increases electron

temperature and ion charge states[26]. Burning voltage and velocity increase in the same manner as ion charge states.

According to the hydrodynamic model, the pressure gradients of electrons and ions, coupled through electron-ion interaction, are driving ion acceleration. Although not exactly applicable to dense plasma, one may use the equilibrium equation of state for plasma to describe the pressure

$$p = nkT - \frac{e^2}{24\pi\varepsilon_0\lambda^3} \tag{10}$$

where the first term is the ideal fluid contribution[38] and the second is a first-order nonideal correction describing the shielded Coulomb interaction of charged particles[39]; $n = n_e + n_i$ is the density of charged particles, and

$$\lambda = \left(\frac{\varepsilon_0 kT}{e^2 n}\right)^{1/2} \tag{11}$$

is the Debye length. The nonideal correction becomes small for plasma of low density. To get an approximation for the pressure gradient along the field lines we use the derivative

$$\nabla p = nk\nabla T + kT\nabla n + \frac{e^3}{48\pi\varepsilon_0^{3/2}}\left[\left(\frac{n}{kT}\right)^{3/2} k\nabla T - \left(\frac{n}{kT}\right)^{1/2}\nabla n\right] \tag{12}$$

The pressure in a magnetic field is actually a tensor whose evaluation is beyond the scope of this discussion. An additional shortcoming of equation (12) is that electron and ion temperatures are increasingly decoupled when the plasma density decreases. It is known that the temperature of electrons decreases from typically 5 eV to 1-2 eV while the concept of temperature is not really applicable to ions due to the non-isotropic ion energy distribution. When the plasma is expanding, the densities of both ions and electrons drop by many orders of magnitude. Therefore, despite the shortcomings of equation (12), we may argue that the term $kT\nabla n$ will give the largest contribution to ion acceleration. Interestingly, a higher temperature due to the magnetic field will increase one factor of this term, namely kT, but it will *decrease* the gradient, ∇n. For free expansion, in the absence of a magnetic field, the density decreases with r^{-2} as a consequence of particle conservation, with r being the distance from the cathode spot. When the plasma motion follows magnetic field lines, the expansion is $n \sim r^{-\alpha}$ with $0 < \alpha < 2$. Therefore, the specifics of ion acceleration will depend on the magnetic field configuration and not only on the field strength.

In addition to these hydrodynamic arguments, one may also consider charged particle motion using the kinetic plasma model. In the absence of collisions (a good approximation only far from the cathode spot), the magnetic moment of a charged particle

$$\mu = \frac{m v_\perp^2}{2\,B} \tag{13}$$

is an adiabatic invariant, leading to what is known as the mirror effect[38]. Depending on whether the field strength decreases or increased, the velocity component perpendicular to the field line decreases or increases, respectively. In the absence of collisions, kinetic energy is conserved and thus the velocity component parallel to the field line increases or decreases, respectively. The force acting on the particle is[38]

$$\mathbf{F}_\parallel = -\mu\frac{\partial B}{\partial \mathbf{s}} \tag{14}$$

where $d\mathbf{s}$ is a line element along **B**. Roughly speaking, the plasma will slow down when streaming into a region of stronger magnetic field, as is the case when using the long coil shown in figure 9, and it will accelerate when it is produced in a high field and streaming into a region of lower field, as is the case when using the short coil of figure 10. This qualitatively explains the results shown in figure 10.

In more complicated situations (e.g. when both the short and long coil are used), we have competing effects such as reduction of ∇n and variation in ∇B, and thus one may expect non-monotonic behavior of ion velocity as a function of field strength, as shown in figure 10.

The fact that kinetic ion energies of vacuum arc plasmas can be manipulated by suitable magnetic field configurations have not been reported before. For energetic deposition of thin films by filtered cathodic arc plasma deposition, the kinetic ion energy is of great importance because it influences film nucleation, the formation of an intermixed layer, subplantation depth, and the kinetics of the growing film. Additionally, film texture and the type of chemical bonds may be influenced. This is particularly important for the deposition of diamond-like carbon films. It is often quoted that a kinetic energy of 50-100 eV/atom is needed to obtain diamond-like film properties (e.g. Ref.[40,41]). A macroparticle filter (used to remove macroparticles from the vacuum arc plasma[42,43]) represents a magnetic field configuration that has an influence on all plasma parameters, including the ion kinetic energy. Therefore, independent ion kinetic energy measurements have been made at our pulsed, high-field Twist-Filter[44] that is used to synthesize ultrathin (3 nm) protective ta-C films on magnetic multilayers[45]. Using the current perturbation techniques described here, we found $E_{kin} \approx 43$ eV for carbon ions. This value is much higher than the 19 eV listed in Table 1 for energy without external magnetic fields. It explains why we have been able to obtain high-quality films that are rich in diamond (sp^3) bonds even without the use of substrate bias.

C. Angular dependence of ion flux parameters

Finally we discuss the angular dependence of the ion flux and kinetic ion energy. Because the angular distribution would greatly depend on the specifics of any magnetic field that is present, we limited the investigation to the case without external magnetic field. Additionally, the position, shape, and area of the anode may have an influence. To minimize anode effects, a cylindrically symmetric chamber was used with the chamber wall as anode and with the plasma source in the center such as that the anode position and area does not change with angle (Fig. 11). As pointed out by Kutzner and Miller[46], there are only few measurements of angular dependence on ion flux distribution and even less for the angular dependence of ion energy.

It is generally assumed[25,47] that the flux can be approximated by a cosine distribution

$$j_i(\vartheta) = j_i(\vartheta = 0) \cdot \cos\vartheta \tag{15}$$

where ϑ is the angle between the flux direction and cathode surface normal, or an even more peaked distribution such as[48]

$$j_i(\vartheta) = j_i(\vartheta = 0) \cdot \cos^2\vartheta \tag{16}$$

Our measurements as shown in figure 13 confirm that the cosine relationship fits well for $\vartheta < 60°$ but the flux is greater for large angles. The flux is less peaked than reported by other researchers[25,47-49]. Most likely, this is due to the more axial position of the anode in the other experiments.

The angular distribution of ion kinetic energy (Fig. 12) shows even larger deviation from a cosine distribution. The measured distribution can rather be fitted by a superposition of an isotropic distribution and a cosine distribution:

$$E_{kin}(\vartheta) = E_{kin,90} + E^*_{kin}(\vartheta = 0) \cdot \cos\vartheta \tag{17}$$

where $E_{kin,90}$ is the kinetic energy of ions moving in the cathode plane, and $E^*_{kin}(\vartheta = 0)$ is the difference to the maximum energy observed at the surface normal, i.e. trivially $E^*_{kin}(\vartheta = 0) = E_{kin}(\vartheta = 0) - E_{kin,90}$. Table 2 gives data for fit constants of selected materials. One can see that the isotropic component is larger than the angle-dependent component.

V. CONCLUSIONS

Although it is true that vacuum arc ion energies are generally of order 10^4 m/s, more detailed investigations of the kinetic ion energy as a function of cathode material, angle to the cathode surface normal, and external magnetic fields give insight to direct relations with other discharge and plasma parameters, such as arc voltage and ion charge state distribution. A large number of ion species were investigated. Due to the simplicity of the measuring method, it is believed that the results obtained here are more reliable than previous measurements. However, the data presented here are not charge-state-resolved and they are averaged over many individual measurements. Magnetic fields are often used to increase ion charge states, and it is shown that the kinetic energy of ions can be increased as well. It is shown that the ion kinetic energy can be *decreased* if the cathode is in a low-field region and the plasma streams into a high-field region. Therefore, a magnetic field can be used to increase or decrease the kinetic ion energy depending on the magnetic field configuration.

ACKNOWLEDGMENTS

We thank Ian Brown and Efim Oks for support of this endeavor. This work was supported by the U.S. Department of Energy, Office of Energy Research, under Contract No. DE-AC03-76SF00098, and by the Russian Foundation for Basic Research, under Grant No. 99-02-18163.

Figure Captions

Figure 1. Schematic of the experimental arrangement using the modified "Mevva V" ion source. A simplified electric schematic shows the pulse-forming-network with the modulating LC branch. The ion current detector is a probe in the ion saturation regime.

Figure 2. Example of the arc voltage (top curve), modulated arc current (bottom curve) and ion beam current (center curve) for tantalum plasma, averaged over 16 discharge pulses.

Figure 3. Delay between corresponding arc current and tantalum ion current extrema is plotted as a function of time after arc ignition (full circles). With the given cathode-probe distance, a time-dependent tantalum ion velocity can be derived (squares).

Figure 4. Arc voltage and ion kinetic energy as a function of magnetic field. Data for individual elements can be found in Table 1.

Figure 5. Cohesive energy of the cathode material (squares) and relative ion erosion rates (circles). The latter were determined by the ion saturation current divided by average ion charge state.

Figure 6. Ion kinetic energy of selected cathode materials as a function of magnetic field strength measured with the experiment of figure 1, with I_{arc} = 250 A and for t > 150 μs.

Figure 7. Burning voltage associated with measurements shown in Figure 6.

Figure 8. Ion kinetic energy as a function of arc burning voltage (data of figures 6 and 7).

Figure 9. Experimental set-up for investigating the influence of the kinetic ion energy on the magnetic field configuration. Two field coils are available; for simplicity, only the power connection of the long coil is shown here.

Figure 10. Kinetic energy of carbon ions for three magnetic field configurations: high-field short coil at cathode (squares), low-field, long coil (circles), both short and long field coil (triangles). For all measurements, the cathode-to-detector distance was kept constant at 515 mm. All coils were operated up to a maximum current of 1150 A. Note that for a given current, the long coil has a much lower field due to its smaller number of turns per length, however, it is influencing a unit volume of moving plasma for a much longer duration than the short coil.

Figure 11. Experimental setup for measuring the angular dependence of ion flux parameters. The rotatable source of plasma (cathode assembly) is placed in the center of a cylindrically symmetric chamber.

Figure 12. Ion kinetic energy for various cathode materials as a function of angle; 0° corresponds to the cathode surface normal. The geometry for this measurement is shown in figure 11. No external magnetic field was applied.

Figure 13. Ion particle flux for various cathode materials as function of angle (compare figures 11 and 12).

Figure 14. Comparison of experimental velocity data with hydrodynamic approximations, eqns. (6) (7).

Figure 15. Cohesive energy, electron temperature, and ion kinetic energy for many elements.

Tables

Table 1 Average ion velocity, and burning voltage, and derived data for most conducting elements of the Periodic Table measured for arc currents 100 – 300 A at pressure 10^{-4} Pa. The result does not noticeable depend on arc current and is valid for pressures up to about 10^{-2} Pa. No external magnetic field was applied. Data are valid for $t > 150$ μs after arc initiation. The cohesive energy is from Kittel[50], the average charge state numbers were taken from Brown[16], the electron temperatures from Anders[18], and all other data are this work.

Symbol	Atomic number	Arc burning voltage (V)	Average ion velocity (m/s)	Kinetic ion energy (eV)	Ion Momentum (10^{-22} kg m/s)	Cohesive energy (eV/atom)	Average ion charge state number	Temperature of electrons (eV)	Approximate Ion Mach Number
Li	3	23.5	23100	19.3	2.67	1.63	1.0	2.0	3.1
C	6	31	17300	18.7	3.45	7.37	1.0	2.0	3.0
Mg	12	18.6	19800	49.4	7.98	1.51	1.5	2.1	4.8
Al	13	22.6	15400	33.1	6.89	3.39	1.7	3.1	3.3
Si	14	21.0	15400	34.5	7.18	4.63	1.4	2.0	4.1
Ca	20	20.5	13900	39.9	10.2	1.84	1.9	2.2	4.2
Sc	21	21.6	14600	49.6	10.9	3.90	1.8	2.4	4.5
Ti	22	22.1	15400	58.9	12.2	4.85	2.1	3.2	4.3
V	23	22.7	16300	70.2	13.8	5.51	2.1	3.4	4.5
Cr	24	22.7	16300	71.6	14.1	4.10	2.1	3.4	4.6
Fe	26	21.7	12600	45.9	11.7	4.28	1.8	3.4	3.7
Co	27	21.8	12100	44.4	11.8	4.39	1.7	3.0	3.8
Ni	28	21.7	11500	40.6	11.2	4.44	1.8	3.0	3.6
Cu	29	22.7	13200	57.4	13.9	3.49	2.0	3.5	4.0
Zn	30	17.1	10300	35.7	11.1	1.35	1.4	2.0	4.2
Ge	32	20.0	11100	46.2	13.4	3.85	2.0	2.0	4.8
Sr	38	18.5	11500	60.5	16.8	1.72	2.0	2.5	4.9
Y	39	19.9	13200	80.3	19.5	4.37	2.3	2.4	5.8
Zr	40	22.7	15400	112	23.3	6.25	2.6	3.7	5.5
Nb	41	27.9	16300	128	25.1	7.57	3.0	4.0	5.6
Mo	42	29.5	17300	149	27.6	6.82	3.1	4.5	5.8
Ru	44	23.8	13900	139	23.3	6.74	2.9	4.5	4.8
Rh	45	23.8	14600	142	24.9	5.75	3.0	4.5	5.1

Pd	46	23.5	12100	80.1	21.4	3.89	1.9	2.0	6.3
Ag	47	22.8	11100	68.7	19.9	2.95	2.1	4.0	4.1
Cd	48	14.7	6800	26.6	12.6	1.16	1.3	2.1	3.6
In	49	16.0	6000	21.6	11.5	2.52	1.4	2.1	3.2
Sn	50	17.4	7000	29.5	13.6	3.13	1.5	2.1	3.7
Ba	56	16.5	7900	44.6	18.0	1.90	2.0	2.3	4.4
La	57	18.7	6900	34.6	16.0	4.47	2.2	1.4	4.9
Ce	58	17.6	7900	45.5	18.4	4.32	2.1	1.7	5.1
Pr	59	20.5	8400	51.5	19.6	3.70	2.2	2.5	4.5
Nd	60	19.2	8100	49.7	19.5	3.40	2.2	1.6	5.6
Sm	62	18.8	8100	51.8	20.3	2.14	2.1	2.2	4.9
Gd	64	20.4	8100	54.1	21.3	4.14	2.2	1.7	5.6
Tb	65	19.6	8400	58.1	22.1	4.05	2.2	2.1	5.3
Dy	66	19.8	8400	59.4	22.6	3.04	2.3	2.4	5.0
Ho	67	20.0	8600	64.1	23.7	3.14	2.3	2.4	5.2
Er	68	19.2	8900	69.3	24.8	3.29	2.4	2.0	5.9
Hf	72	23.3	10300	97.5	30.4	6.44	2.9	3.6	5.2
Ta	73	28.6	12000	136	36.2	8.10	2.9	3.7	6.0
W	74	28.7	11100	117	33.6	8.90	3.1	4.3	5.2
Ir	77	25.5	10700	113	34.1	6.94	2.7	4.2	5.2
Pt	78	23.7	8100	67.2	26.4	5.84	2.1	4.0	4.1
Au	79	19.7	6900	49.0	22.6	3.81	2.0	4.0	3.5
Pb	82	17.3	5800	35.8	19.8	2.03	1.6	2.0	4.2
Bi	83	14.4	4700	23.9	16.3	2.18	1.2	1.8	3.6

Table 2
Fit constants to be used with equation (17), describing the angular dependence of the kinetic ion energy for selected materials.

Ion species	$E_{kin,90}$, (eV)	$E^{*}_{kin}(\vartheta = 0)$, (eV)
C	15	4
Mg	32	17
Ti	42	18
Cu	42	15
Ag	48	21
Ta	96	40
Pb	27	12
Bi	20	4

References

[1] J. M. Lafferty, *Vacuum Arcs – Theory and Applications* (Wiley, New York, 1980).

[2] G. A. Mesyats and D. I. Proskurovsky, *Pulsed Electrical Discharge in Vacuum* (Springer-Verlag, Berlin, 1989).

[3] A. Anders, S. Anders, B. Jüttner, W. Bötticher, H. Lück, and G. Schröder, IEEE Trans. Plasma Sci. **20**, 466-472 (1992).

[4] B. Jüttner, V. F. Puchkarev, E. Hantzsche, and I. Beilis, *Cathode Spots,* in *Handbook of Vacuum Arc Science and Technology*, edited by R. L. Boxman, D. M. Sanders, and P. J. Martin (Noyes, Park Ridge, New Jersey, 1995), p. 73-281.

[5] G. A. Mesyats, *Cathode Phenomena in a Vacuum Discharge: The Breakdown, the Spark, and the Arc* (Nauka, Moscow, Russia, 2000).

[6] G. Y. Yushkov, A. Anders, E. M. Oks, and I. G. Brown, J. Appl. Phys. **88**, 5618-5622 (2000).

[7] A. Schuster, Nature **57**, 17 (1897).

[8] W. Feddersen, Annalen der Physik und Chemie **113**, 437-467 (1861).

[9] R. Tanberg, Phys. Rev. **35**, 1080-1089 (1930).

[10] A. A. Plyutto, V. N. Ryzhkov, and A. T. Kapin, Sov. Phys. JETP **20**, 328-337 (1965).

[11] W. D. Davis and H. C. Miller, J. Appl. Phys. **40**, 2212-2221 (1969).

[12] A. S. Bugaev, V. I. Gushenets, A. G. Nikolaev, E. M. Oks, and G. Y. Yushkov, IEEE Trans. Plasma Sci. **27**, 882-887 (1999).

[13] A. S. Bugaev, E. M. Oks, G. Y. Yushkov, A. Anders, and I. G. Brown, Rev. Sci. Instrum. **71**, 701-703 (2000).

[14] G. Y. Yushkov, E. M. Oks, A. Anders, and I. G. Brown, J. Appl. Phys. **87**, 8345-8350 (2000).

[15] G. Yushkov, *Measurements of directed ion velocity in vacuum arc plasmas by arc current perturbation*, IXX Int. Symp. on Discharges and Electrical Insulation in Vacuum, Xi'an, P.R. China, 2000, p. 260-263.

[16] I. G. Brown, Rev. Sci. Instrum. **65**, 3061-3081 (1994).

[17] R. J. Goldston and P. H. Rutherford, *Introduction to Plasma Physics* (Institute of Physics, Bristol, 1997).

[18] A. Anders, Phys. Rev. E **55**, 969-981 (1997).

[19] A. Anders, B. Yotsombat, and R. Binder, J. Appl. Phys. **89**, June (2001).

[20] A. Anders, Appl. Phys. Lett. **78**, 2837-2839 (2001).

[21] E. M. Oks, A. Anders, I. G. Brown, M. R. Dickinson, and R. A. MacGill, Nucl. Instrum. Meth. Meth. Phys. Res. B **127/128**, 779-781 (1997).

[22] C. Wieckert, Contrib. Plasma Phys. **27**, 309-330 (1987).

[23] E. Hantzsche, IEEE Trans. Plasma Sci. **23**, 893-898 (1995).

[24] A. Anders, Surf. & Coat. Technol. **136**, 85-92 (2001).

[25] H. C. Miller and J. Kutzner, Contrib. Plasma Phys. **31**, 261-277 (1991).

[26] E. M. Oks, A. Anders, I. G. Brown, M. R. Dickinson, and R. A. MacGill, IEEE Trans. Plasma Sci. **24**, 1174-1183 (1996).

[27] A. Anders, B. Yotsombat, and R. Binder, J. Appl. Phys. **89**, 7764-7771 (2001).

[28] E. A. Litvinov, *Kinetic of cathode jet at explosive emission of electrons,* in *High Current Nanosecond Pulsed Sources of Accelerated Electrons (in Russian)* (Nauka, Novosibirsk, 1974).

[29] E. Hantzsche, IEEE Trans. Plasma Sci. **34**, 34-41 (1992).

[30] I. A. Krinberg and M. P. Lukovnikova, J. Phys. D: Appl. Phys. **29**, 2901-2906 (1996).
[31] G. Y. Yushkov, A. S. Bugaev, I. A. Krinberg, and E. M. Oks, Doklady Physics **46**, 307-309 (2001).
[32] I. A. Krinberg, Techn. Phys. **46**, no. 11 in print (2001).
[33] A. Anders, IEEE Trans. Plasma Sci. **27**, 1060-1067 (1999).
[34] K. Tsuruta, K. Skiya, and G. Watanabe, IEEE Trans. Plasma Sci. **25**, 603-608 (1997).
[35] A. Anders, presented at 7th EVC, Madrid, Sept. 2001, to be published in VACUUM (2001).
[36] I. G. Brown and H. Shiraishi, IEEE Trans. Plasma Sci. **18**, 170-171 (1990).
[37] S. Anders, A. Anders, K. M. Yu, X. Y. Yao, and I. G. Brown, IEEE Trans. Plasma Sci. **21**, 440-446 (1993).
[38] F. F. Chen, *Plasma Physics and Controlled Fusion* (Plenum Press, New York, 1984).
[39] K. Günther and R. Radtke, *Electric Properties of Weakly Nonideal Plasmas* (Akademie-Verlag, Berlin, 1984).
[40] J. Robertson, Diamond & Rel. Mat. **2**, 984-989 (1993).
[41] G. M. Pharr, D. L. Callahan, D. McAdams, T. Y. Tsui, S. Anders, A. Anders, J. W. Ager, I. G. Brown, C. S. Bhatia, S. R. P. Silva, and J. Robertson, Appl. Phys. Lett. **68**, 779-781 (1996).
[42] I. I. Aksenov, V. A. Belous, and V. G. Padalka, Instrum. Exp. Tech. **21**, 1416-1418 (1978).
[43] A. Anders, Surf. & Coat. Technol. **120-121**, 319-330 (1999).
[44] A. Anders and R. A. MacGill, Surf. & Coat. Technol. **133-134**, 96-100 (2000).
[45] A. Anders, W. Fong, A. Kulkarni, F. R. Ryan, and C. S. Bhatia, IEEE Trans. of Plasma Sci. **29**, in print (2001).
[46] J. Kutzner and H. C. Miller, J. Phys. D: Appl. Phys. **25**, 686-693 (1992).
[47] J. V. R. Heberlein and D. Porto, IEEE Trans. of Plasma Sci. **11**, 152-159 (1983).
[48] V. M. Khoroshikh, I. I. Aksenov, and I. I. Konovalov, Sov. Phys. - Techn. Phys. **33**, 723-724 (1988).
[49] D. T. Tuma, C. L. Chen, and D. K. Davis, J. Appl. Phys. **49**, 3821-3831 (1978).
[50] C. Kittel, *Introduction to Solid State Physics* (John Wiley & Sons, New York, 1986).

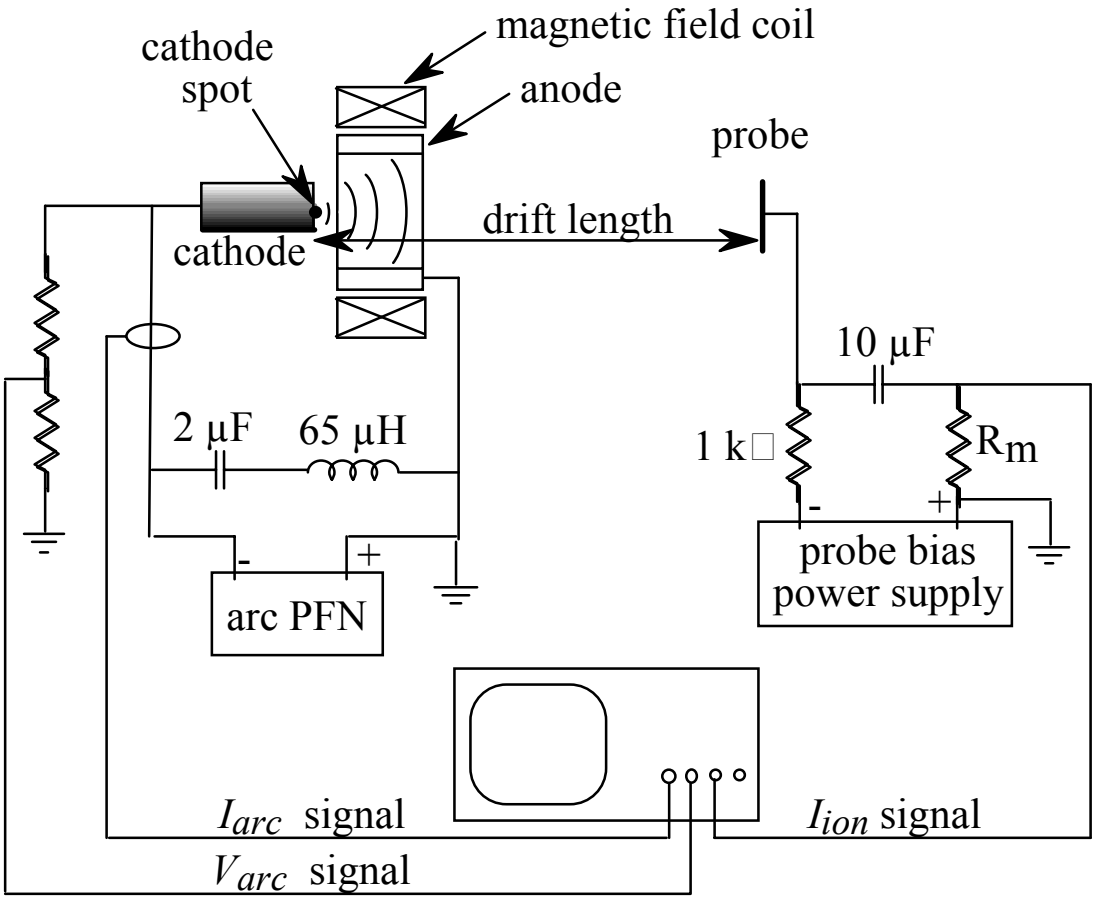
magnetic field coil
cathode
spot
anode
probe
drift length
cathode
10 μF
2 μF
65 μH
1 k□
Rm
-
+
-
+
probe bias
power supply
arc PFN
Iarc signal
Varc signal
Iion signal

Figure 1

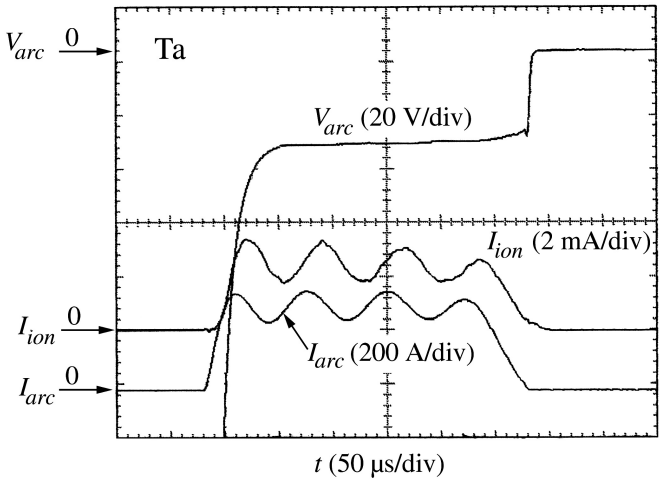
V_{arc} 0
Ta
V_{arc} (20 V/div)
I_{ion} (2 mA/div)
I_{ion} 0
I_{arc} (200 A/div)
I_{arc} 0
t (50 μs/div)

Figure 2

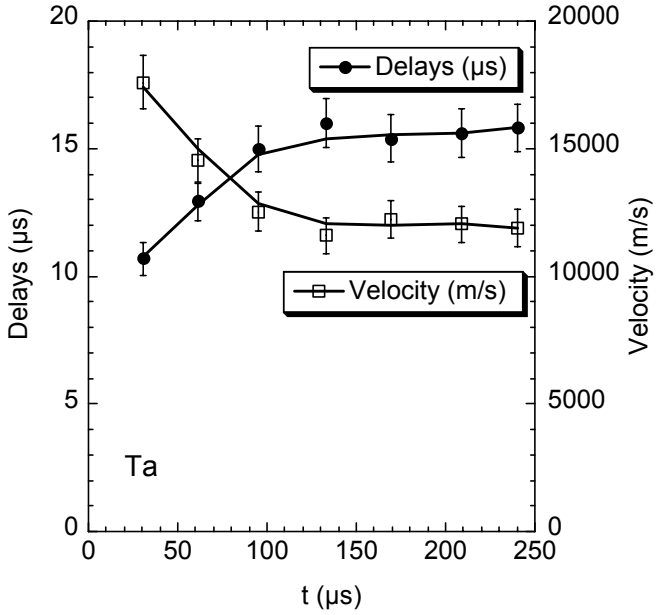
Delays (μs)
Velocity (m/s)
Ta
t (μs)
0
5
10
15
20
0
5000
10000
15000
20000
0
50
100
150
200
250

Figure 3

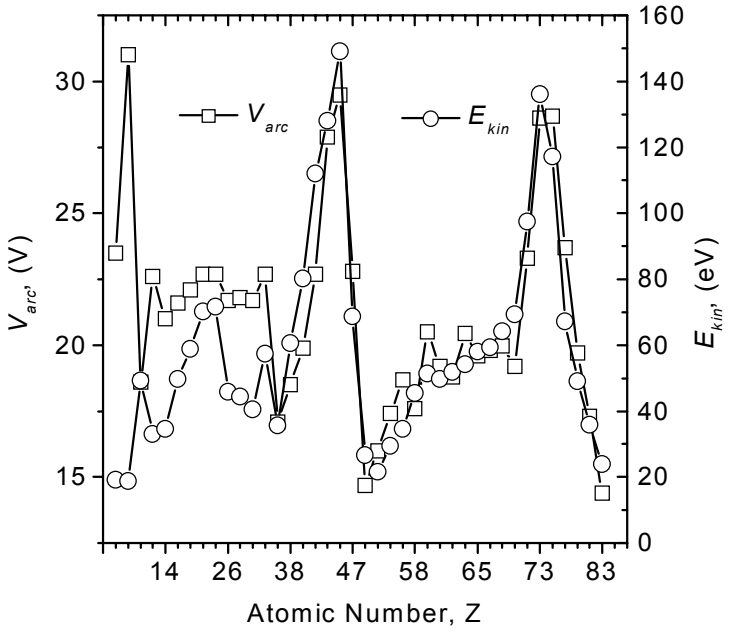
V_{arc}
E_{kin}
V_{arc}, (V)
E_{kin}, (eV)
Atomic Number, Z
30
25
20
15
160
140
120
100
80
60
40
20
0
14
26
38
47
58
65
73
83

Figure 4

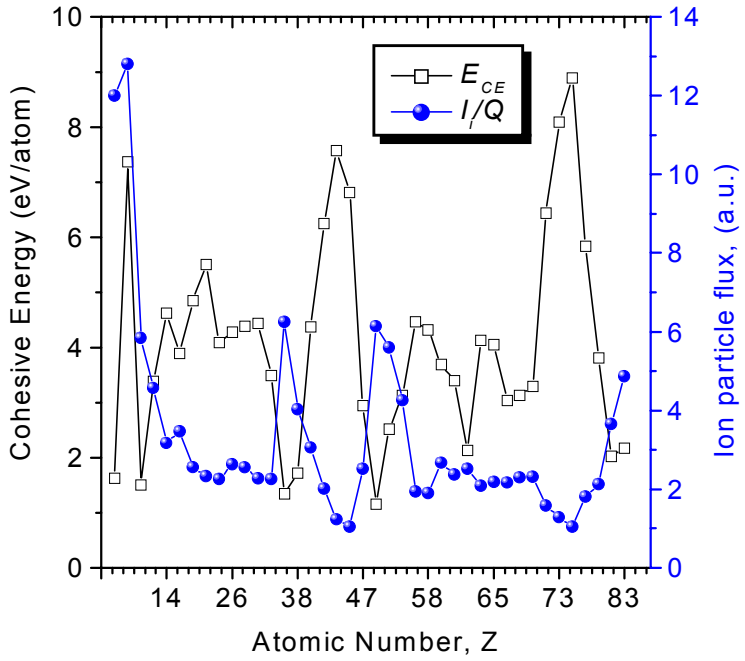
Cohesive Energy (eV/atom)
Ion particle flux, (a.u.)
Atomic Number, Z
E_{CE}
I_i/Q
0
2
4
6
8
10
12
14
14
26
38
47
58
65
73
83

Figure 5

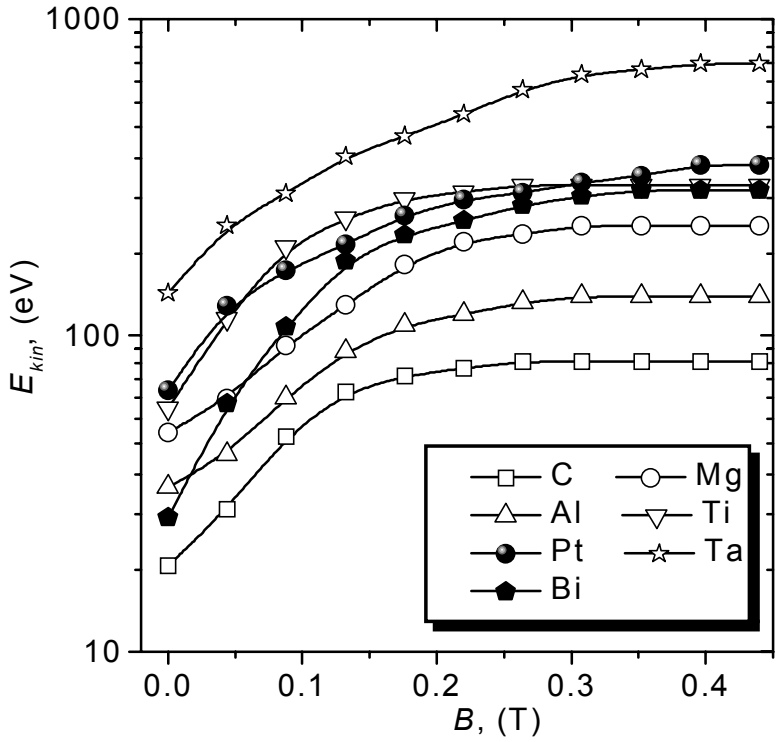

Figure 6

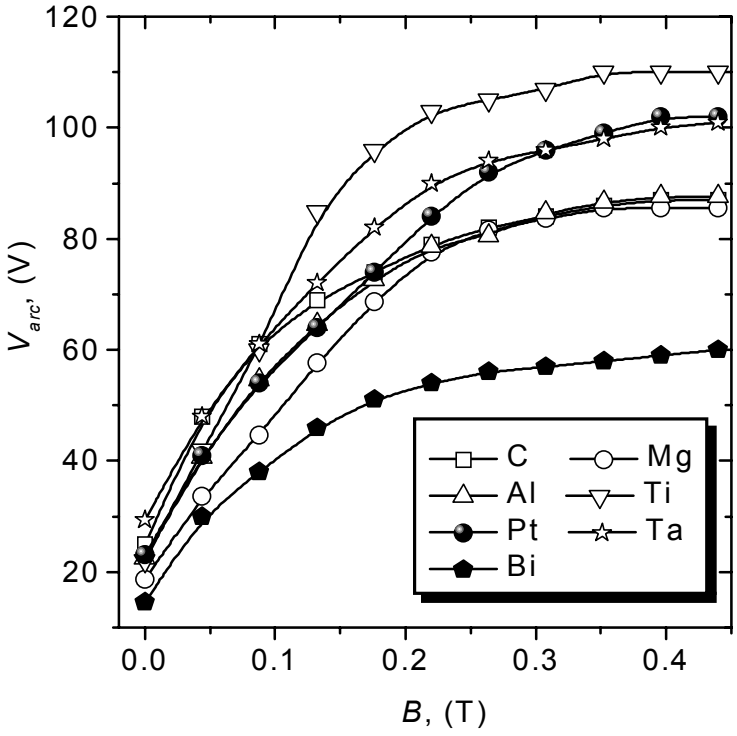

Figure 7

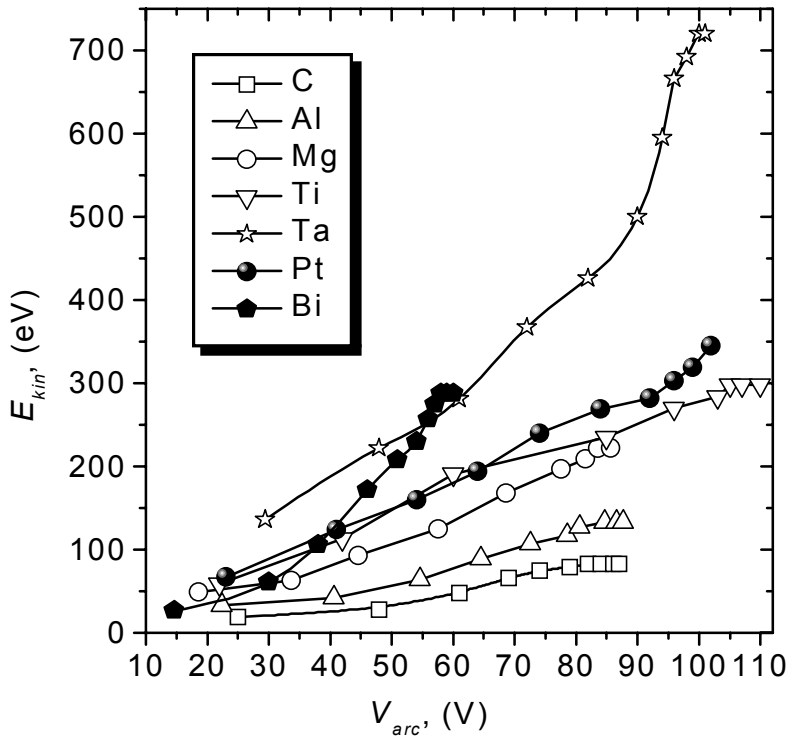
C
Al
Mg
Ti
Ta
Pt
Bi
E_{kin}, (eV)
V_{arc}, (V)
0
100
200
300
400
500
600
700
10
20
30
40
50
60
70
80
90
100
110

Figure 8

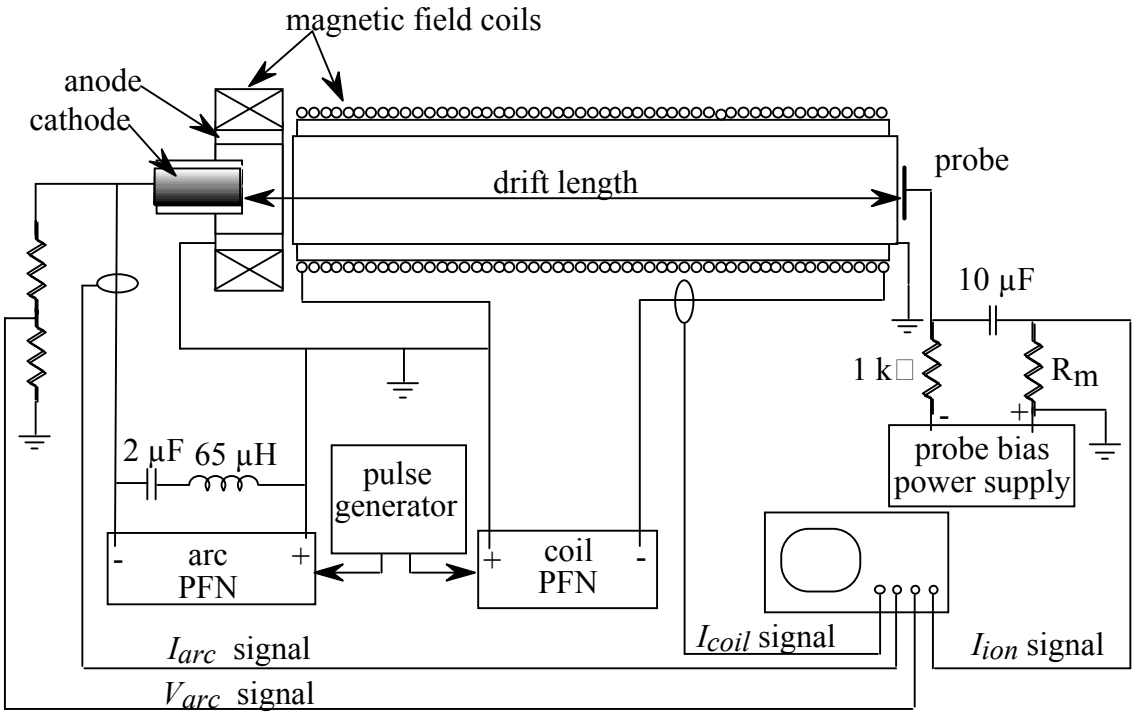
magnetic field coils
anode
cathode
drift length
probe
10 μF
1 kΩ
Rm
2 μF
65 μH
pulse generator
probe bias power supply
arc PFN
coil PFN
Icoil signal
Iion signal
Iarc signal
Varc signal

Figure 9

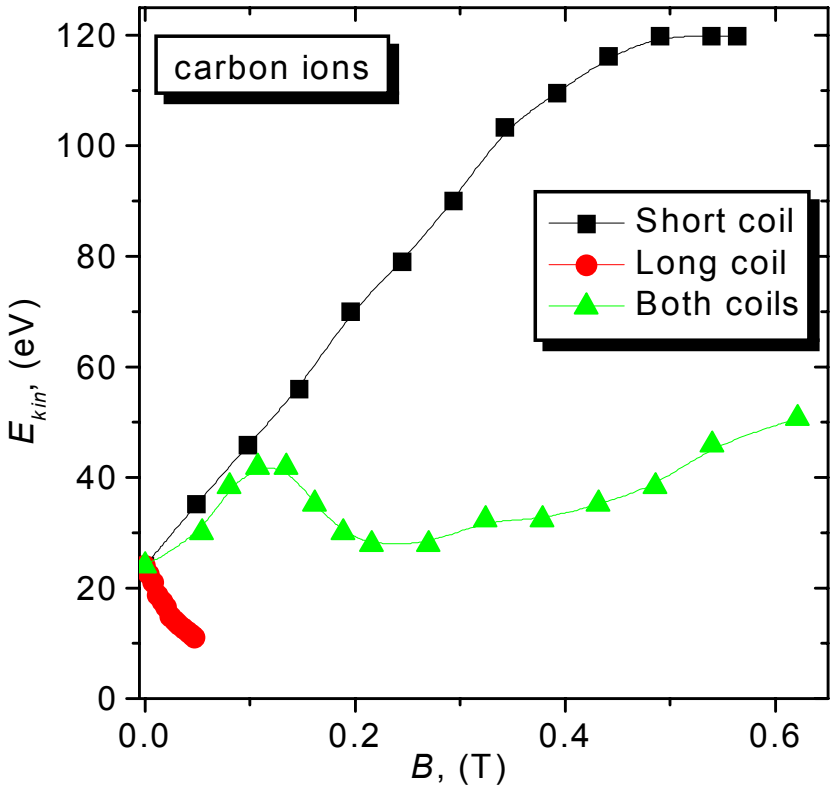
carbon ions
Short coil
Long coil
Both coils
E_{kin}, (eV)
B, (T)
0
20
40
60
80
100
120
0.0
0.2
0.4
0.6

Figure 10

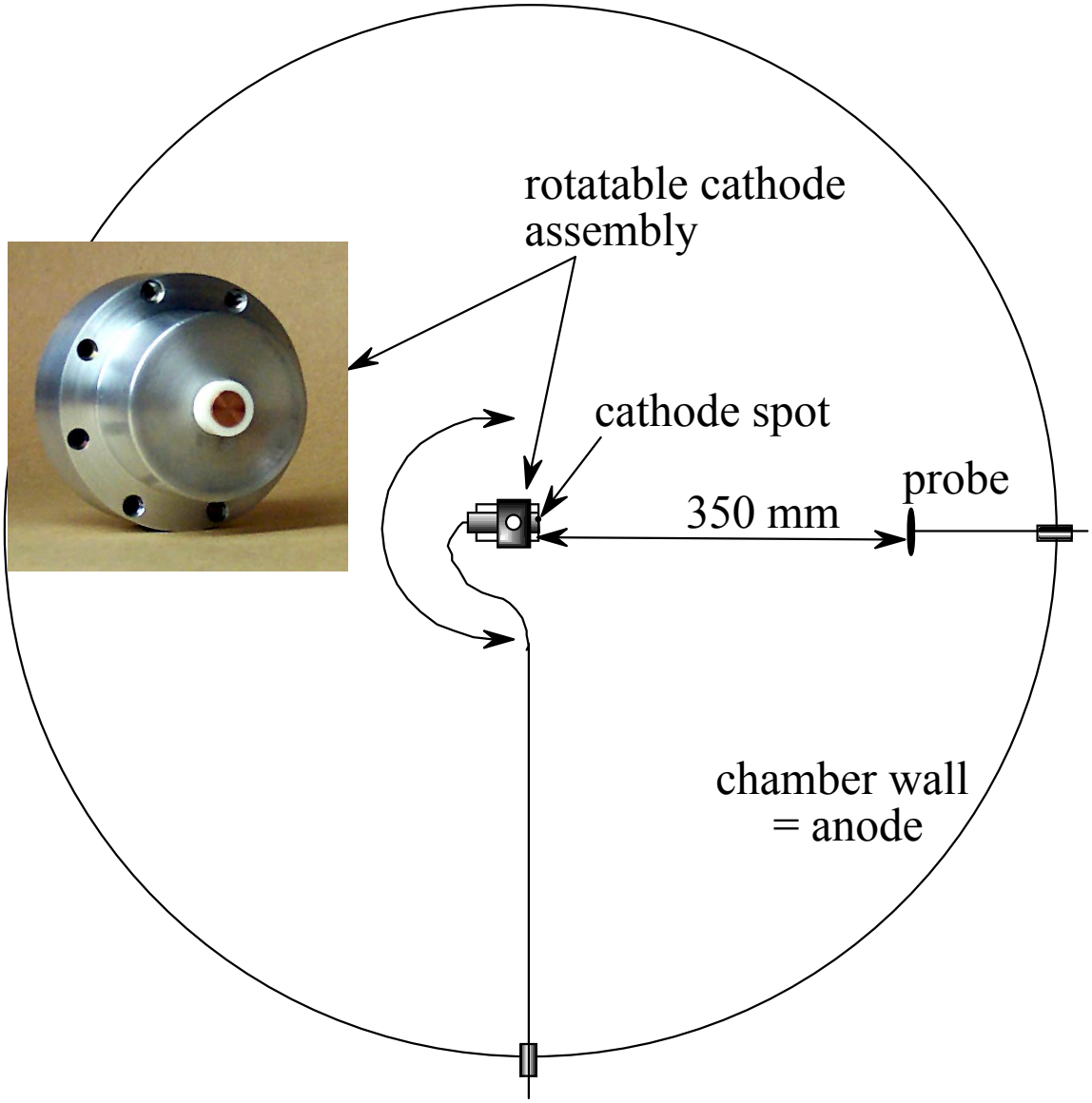
rotatable cathode
assembly
cathode spot
probe
350 mm
chamber wall
= anode

Figure 11

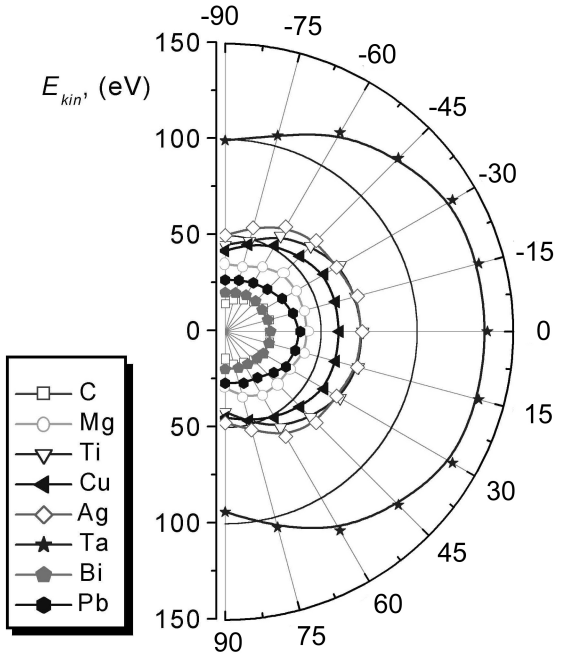
E_{kin}, (eV)
-90
-75
-60
-45
-30
-15
0
15
30
45
60
75
90
150
100
50
0
50
100
150
C
Mg
Ti
Cu
Ag
Ta
Bi
Pb

Figure 12

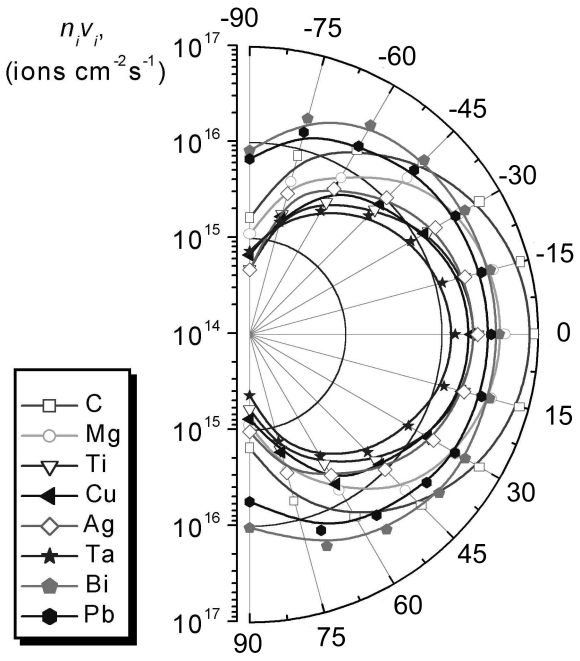
$n_i v_i$,
(ions cm^{-2}s^{-1})
10^{17}
10^{16}
10^{15}
10^{14}
10^{15}
10^{16}
10^{17}
-90
-75
-60
-45
-30
-15
0
15
30
45
60
75
90
C
Mg
Ti
Cu
Ag
Ta
Bi
Pb

Figure 13

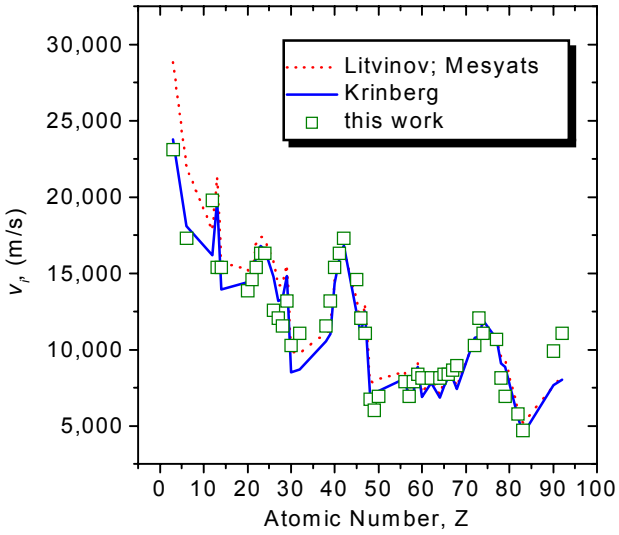
30,000
25,000
20,000
15,000
10,000
5,000
v_r (m/s)
0
10
20
30
40
50
60
70
80
90
100
Atomic Number, Z
Litvinov; Mesyats
Krinberg
this work

Figure 14

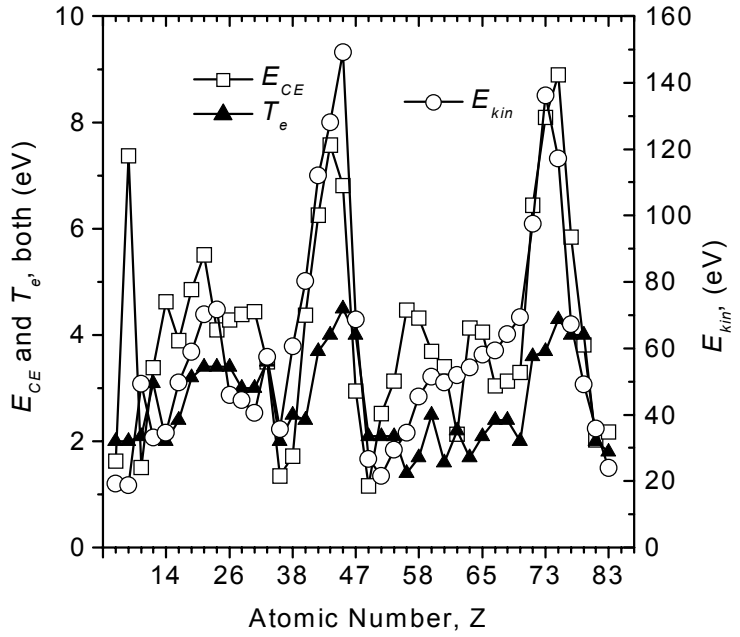
E_{CE}
T_e
E_{kin}
E_{CE} and T_e, both (eV)
E_{kin}, (eV)
Atomic Number, Z
0
2
4
6
8
10
0
20
40
60
80
100
120
140
160
14
26
38
47
58
65
73
83

Figure 15